Theor Chem Acc (2007) 117:1121–1129
DOI 10.1007/s00214-006-0226-x

REGULAR ARTICLE

A gate mechanism indicated in the selectivity filter of the potassium channel KscA

J. Kóňa · M. Minozzi · V. Torre · P. Carloni

Received: 30 August 2006 / Accepted: 13 October 2006 / Published online: 13 January 2007

Abstract Classical molecular dynamics (MD) and non-equilibrium steered molecular dynamics (SMD) simulations were performed on the molecular structure of the potassium channel KcsA using the GROMOS 87 force fields. Our simulations focused on mechanistic and dynamic properties of the permeation of potassium ions through the selectivity filter of the channel. According to the SMD simulations a concerted movement of ions inside the selectivity filter from the cavity to extracellular side depends on the conformation of the peptide linkage between Val76 and Gly77 residues in one subunit of the channel. In SMD simulations, if the carbonyl oxygen of Val76 is positioned toward the ion bound at the S3 site (gate-opened conformation) the net flux of ions through the filter is observed. When the carbonyl oxygen leaped out from the filter (gate-closed conformation), ions were blocked at the S3 site and no flux occurred. A reorientation of the Thr75-Val76 linkage indicated by the CHARMM-based MD simulations performed Berneche and Roux [(2005) Structure 13:591–600; (2000) Biophys J 78:2900–2917] as a concomitant process of the Val76-Gly77 conformational interconversion was not observed in our GROMOS-based MD simulations.

Keywords Channels · Ion transport · Molecular dynamics simulations · Computer modeling · GROMOS

J. Kóňa · M. Minozzi · V. Torre · P. Carloni (✉)
International School for Advanced Studies (SISSA),
Via Beirut 4, 34014 Trieste, Italy
e-mail: carloni@sissa.it

1 Introduction

Potassium channels are passive transport devices enabling ions to flow rapidly through membranes in a thermodynamically downhill direction, which in living cells is from intracellular to extracellular environments. Potassium channels underlie major cellular processes such as electrical excitability, cell volume regulation and hormone secretion [1–3]. High selectivity and rapid transmission of K^+ ions at rates approaching the diffusion limit (ca. 10^7 ions channel^{-1} s^{-1}) are unique properties of potassium channels [4–7].

There are two major classes of K^+ channels: the six-transmembrane-helix voltage gated K^+ channels (Kv) and the two-transmembrane-helix inward-rectifier channels (Kir) [2,3]. The determination of the structure of the bacterial potassium KcsA channel – a member of the Kir class – from *Streptomyces lividans* by MacKinnon and coworkers offered the first molecular view of the general architecture of these membrane proteins [8,9]. The molecular structure of the KcsA channel is composed of three functional parts that include a "gate" on the inner surface of the cell, a "cavity" of diameter of approximately 10 Å in the middle of the channel, and a narrow 12 Å "selectivity filter" leading outside the cell (Fig. 1). The selectivity filter with two conserved glycine residues in TVGYG sequence motif catalyses the dehydration, transfer and rehydration of a K^+ ion. It prevents the passage of Na^+ ions but allows K^+ ions to conduct across the membranes in some ten nanoseconds [5,6,10]. The molecular structure of the pore of the KcsA channel is very similar to that of mammalian voltage gated K^+ channels as demonstrated by the recently determined crystal structure [11]. Therefore the analysis of ionic conduction

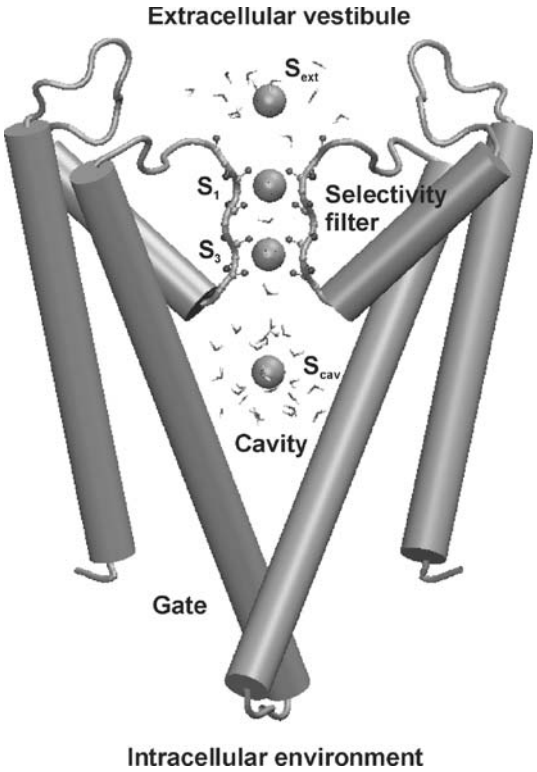

Fig. 1 Schematic drawing of the crystal structure of the close state of the integral domain of the bacterial potassium KcsA channel from *Streptomyces lividans*. For clarity, only two subunits of the tetramer (*cartoon*) are visualized with backbone atoms of the TVGYG sequence motif of the selectivity filter (*ball and stick*). The potassium ions (*VDW ball*) in the 1,3 configuration are bound at the S_{ext}, S_1, S_3 and S_{cav} sites. The ions in the cavity and extracellular vestibule are solvated by water molecules (*tube*)

in the KcsA channel is likely to be relevant to understand the ion permeation along potassium channels in general.

In the X-ray structure of KcsA [9] solved at 2.0 Å resolution at the temperature of 100 K at high K^+ ion concentration (200 mM K^+), four ion binding sites within the filter were identified (sites S_1 to S_4, see also Fig. 1). Thus, when a K^+ ion is located in the filter, its coordination shell consists of eight backbone carbonyl groups (at the S_1, S_2 and S_3 sites) or four carbonyls and four threonine hydroxyl groups (at the S_4 site). The oxygen-K^+ coordination distances range from 2.7 to 3.08 Å, with a mean value of 2.85 Å [9]. Two additional binding sites for permeating ions (S_0 and S_{ext}) were revealed at the boundaries of the filter. The K^+ ion binds at S_0 to four backbone carbonyl oxygens and four water oxygens, while at S_{ext} K^+ ion is fully hydrated, i.e., coordinates with eight water oxygens. The higher resolution structure also resolves a single K^+ ion within the central cavity, solvated by eight water molecules in a square anti-prism arrangement.

Current measurements with K^+ ions led to conclusion that the selectivity filter usually contains two K^+ ions separated by one water molecule [10]. The two ions move in a concerted fashion between two configurations, 1,3 configuration ($S_{ext}^{K+} S_0^{H_2O} S_1^{K+} S_2^{H_2O} S_3^{K+} S_4^{H_2O} S_{cav}^{K+}$) and 2,4 configuration ($S_{ext}^{H_2O} S_0^{K+} S_1^{H_2O} S_2^{K+} S_3^{H_2O} S_4^{K+} S_{cav}^{K+}$), until a third ion enters, displacing the ion on the opposite side of the queue. The free energy difference between the 1,3 and 2,4 configurations is close to zero [10] with an overall free energy barrier of 2–3 kcal/mol [12].

Molecular dynamics (MD) simulations have provided very important insights on this process [12–38]. In particular, umbrella sampling MD simulations [12,13] based on the CHARMM-PARAM22 force field [39,40] have suggested that: (1) the permeation of potassium ions through the selectivity filter depends on two conformational states of the selectivity filter; (2) the conformational interconversion from conducting to non-conducting state consists of two steps involving the reorientation of the Va76-Gly77 and Thr75-Va76 peptide linkages in one subunit of the tetramer of the selectivity filter; (3) free energy barriers are higher ca. 2–3 kcal/mol for the ion permeation through a non-conducting state than for conducting one.

In a conducting state analogous to the crystal structure at the high K^+ ion concentration [9], the ion bound at the S_3 site is coordinated with carbonyl oxygens of four Val76 and four Thr75 residues. After transition to a non-conducting state, the ion coordinates with carbonyl oxygens of three Val76, four Thr75 and one hydroxyl oxygen of Thr75 [14]. The new state is non-conducting as it is associated to an increase of 2–3 kcal/mol [12,13], which represents a reduction of the permeation by at least two orders of magnitude. Thus, reorientation of the Val76-Gly77 peptide bond has the ability to act as a gate that can effectively block the pore [13]. Although the reorientation of the Val76-Gly77 peptide linkage has also been observed in several independent MD studies of potassium channels based on different force fields and simulation methodologies [14,25–27,29,30], the stabilization of the non-conducting state by the conformational interconversion of the Thr75-Val76 linkage was only indicated in the MD simulations with CHARMM–PARAM22 force field [39,40].

Here we investigated the transition from the 1K_3K to the 2K_4K state using non-equilibrium steered molecular dynamics (SMD) simulations [41–44], using a computational protocol different from that of Berneche and Roux [12–14,24], to provide further insights into mechanistic and dynamic properties of the ion permeation through the selectivity filter of potassium channels.

We monitored trajectories of ion transports from the cavity of KcsA to the extracellular environment in the

conducting and non-conducting state by means of SMD simulations, the approach successfully applied [45–47] for channel systems as the bovine aquaporin-1 [48], aquaglyceroporin GlpF [49] or voltage-gated potassium channel KvAP [50]. By pulling the ion from the S_1 site into extracellular environment we observed the conformational interconversion of the Val76-Gly77 peptide bond with the absence of a change of the Thr75-Val76 linkage, and subsequent blocking of the selectivity filter. On the other hand, in conducting state a concerted movement of the ions took place.

2 Computational details

2.1 Structural model

All MD simulations were based on a crystal structure (PDB ID: 1K4C) of the close state of the integral domain of the bacterial potassium KcsA channel from *Streptomyces lividans* at high K^+ ion concentration [9]. The OCT membrane model was used in simulations, where the channel was embedded in a water/ *n*-octane bilayer enclosed in a box of $70 \times 70 \times 97\,A^3$. The cytoplasm/ membrane environment of the channel simulated by the water/ *n*-octane bilayer supplies a stable hydrofilic/ hydrofobic liquid interface quickly adaptable to the protein structure and has been already successfully reported in the literature [28].

The water–hydrocarbon interfaces were located between Trp87 and Thr85 (extracellular side) and between Trp113 and Arg117 (intracellular side). This choice suggested by Doyle et al. [8] turns out to be in excellent agreement with recent EPR data [51].

In the simulations the ionization state for most residues of the channel was considered to be natural at physiological pH. The His25 and all Asp, Glu, Lys and Arg residues in each subunit of the tetramer of KcsA were simulated in ionic forms except for Glu71. The side chain of Glu71 was constructed in protonated state to form a diacid hydrogen bond with the carboxylate group of Asp80 [31,52,53].

Two stable configurations based on experimental [9,10] and theoretical works [31,32] were simulated: $1K\_3K(S_1^{K+}S_3^{K+}S_{cav}^{K+})$ and $2K\_4K(S_2^{K+}S_4^{K+}S_{cav}^{K+})$. In addition, 4 K^+ and 24 Cl^- counterions were added to make the system charge neutral and simulate 150 mM ion concentration used in the experimental work [9].

2.2 MD simulations

Simulations with the OCT model were performed with the standard GROMOS 87 force field [54,55] by means of the GROMACS-LBM 3.2.1 [56,57] program package. The Berendsen algorithm [58] for temperature and Parrinello-Rahman algorithm for pressure coupling with coupling constants of $\tau_t = 1.0$ ps and $\tau_p = 1.0$ ps were used at a constant temperature (300 K) and pressure (101.325 kPa). The force field parameters derived by Aqvist [59], OPLS [60] and SCP [61] force fields were used for the K^+ ions, *n*-octane and water, respectively. Periodic boundary conditions were used together with PME method [62] for treating long range electrostatics. A time step of 1.0 fs and the LINCS algorithm [63] to constrain bonds involving hydrogens were used along simulations with a 10 Å nonbonded cutoff and the nonbonded pairlist updated every 10 time steps. The simulations were carried out to 2 ns and coordinates were saved for analysis every 1 ps.

The Coulomb interactions are calculated using the GROMACS analysis program (g_energy), which allows to determine long and short range electrostatic interactions as well as the so-called exclusions and 1–4 interactions (first neighbours, second neighbours and third neighbours interactions) as implemented in the GROMOS 87 force field. We calculated long and short range electrostatic interactions between the leaping Val76-Gly77 peptide linkage and residues within ca 5 Å from the linkage (Glu71, Thr72, Thr74, Thr75, Tyr78, Met96 from the subunit A with the leaping Val76-Gly77 peptide linkage; Thr75, Val76 and Gly77 from the neighbouring subunit B; H_2O at the S_2 site and two K^+ ions at S_1 and S_3 sites, see also Fig. 3C), and the rest of the channel and its environment. The 1–4 interactions are neglected.

2.3 Non-equilibrium SMD simulations

Non-equilibrium SMD simulations [41–44] were performed with the same setup as for the GROMOS-based calculations. The SMD simulations were carried out as follows: in the 1K_3K configuration one potassium ion was pulled by artificial harmonic spring along the selectivity filter (*Z* axis) from the S_1 site to extracellular solution ($S_1 \rightarrow S_0 \rightarrow S_{ext} \rightarrow$ extracellular solution) with a steering velocity, $v = 0.03$ Å ps^{-1}.

This value of the velocity was chosen to move the ion 15 Å from the S_1 site into the extracellular solution during 500 ps, and it is ca. 100 fold higher compared to that of the corresponding process in vivo (ca. 10^7 ions $channel^{-1}$ s^{-1}) [22].

The following force constants of harmonic potential were tested: $f_1 = 2.4$, $f_2 = 3.1$ and $f_3 = 4.3$ kcal/mol Å^2 (in preliminary SMD simulations with values smaller than f_1 the pulled ion was not able to follow the artificial spring and kept at the starting S_1 site during the simulated time). For every set of the simulations five

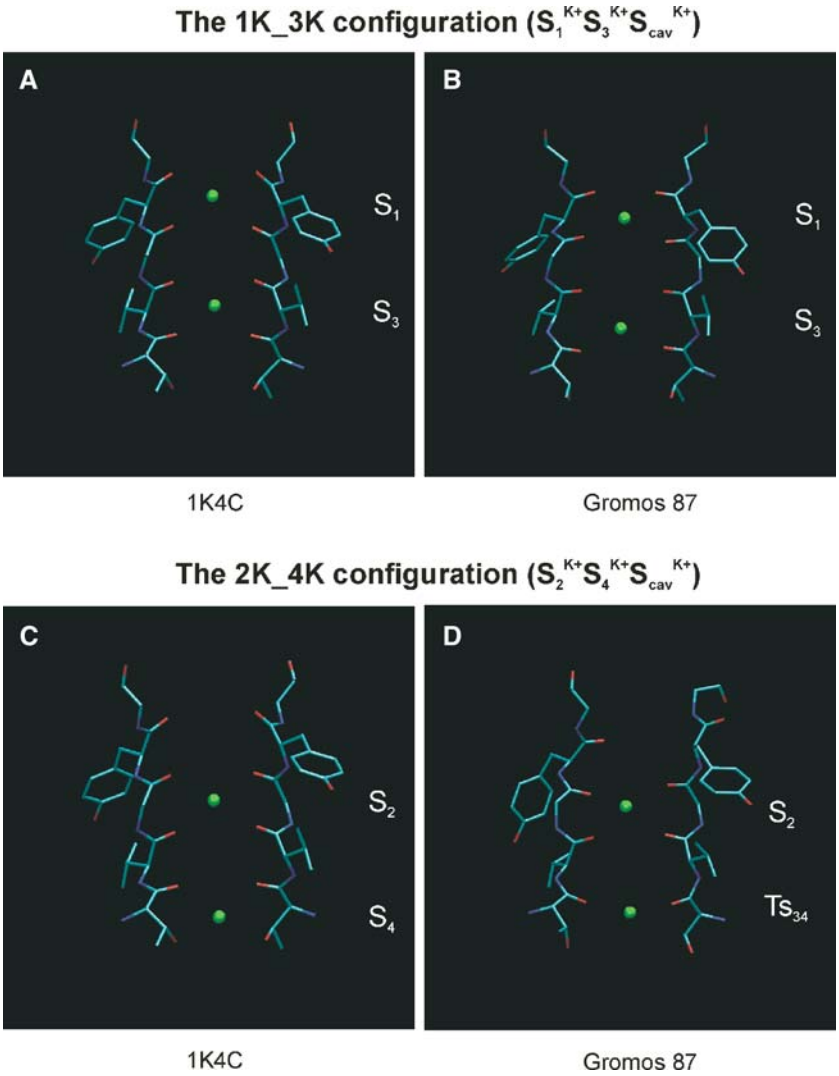

Fig. 2 Snapshots of equilibrated structures from 1 ns MD simulations started from the crystal structure 1K4C, (**A**) the 1K_3K ($S_1^{K+}S_3^{K+}S_{cav}^{K+}$) and (**C**) the 2K_4K configuration ($S_2^{K+}S_4^{K+}S_{cav}^{K+}$). After the 1 ns simulations the GROMOS 87 force field reproduces 1K_3K in accordance with the crystal structure (**B**), whereas 2K_4K is predicted as $S_2^{K+}TS_{34}^{K+}S_{cav}^{K+}$ (**D**). For clarity, hydrogens, water molecules and potassium ions at the S_{cav}, S_0 and S_{ext} sites are not visualized

SMD trajectories were performed, in which the starting structures were taken from snapshots of equilibrium MD simulations.

3 Results and discussion

3.1 MD simulations

We equilibrated two configurations, 1K_3K and 2K_4K started from the geometries of the crystal structure 1K4C (snapshots **A** and **D** in Fig. 2). The GROMOS-based simulations were in good agreement with initial configurations (snapshots **B** and **D** of Fig. 2), however, the K^+ ion at S_4 in the 2K_4K state turned out to be stabilized with stronger ion–dipole interactions with carbonyl oxygens of Thr75 rather than with both carbonyl and hydroxyl oxygens of Thr75.

Within the timescale investigated (2 ns), an interconversion of the Val76-Gly77 peptide bond of one subunit of the channel occurred several times in the 1K_3K configuration with a concomitant fluctuation of the Tyr78-Gly79 linkage at the same subunit of the channel (Charts **A** and **B** in Fig. 3). The conducting conformation, at which the amide nitrogen of Gly77 is positioned away and carbonyl oxygen of Val76 toward a potassium ion bound at the S_3 site, was proposed as a gate-opened conformation, which allows the net flux of ions through the selectivity filter [13]. In the non-conducting state, there is an opposite conformation with the amide nitrogen positioned inside and carbonyl oxygen leaped out from the selectivity filter (gate-closed conformation). The fast fluctuation of the Val76-Gly77 linkage is consistent with a calculation of the free energy barrier associated to such interconversion of only 0.5 kcal/mol at 315 K [13].

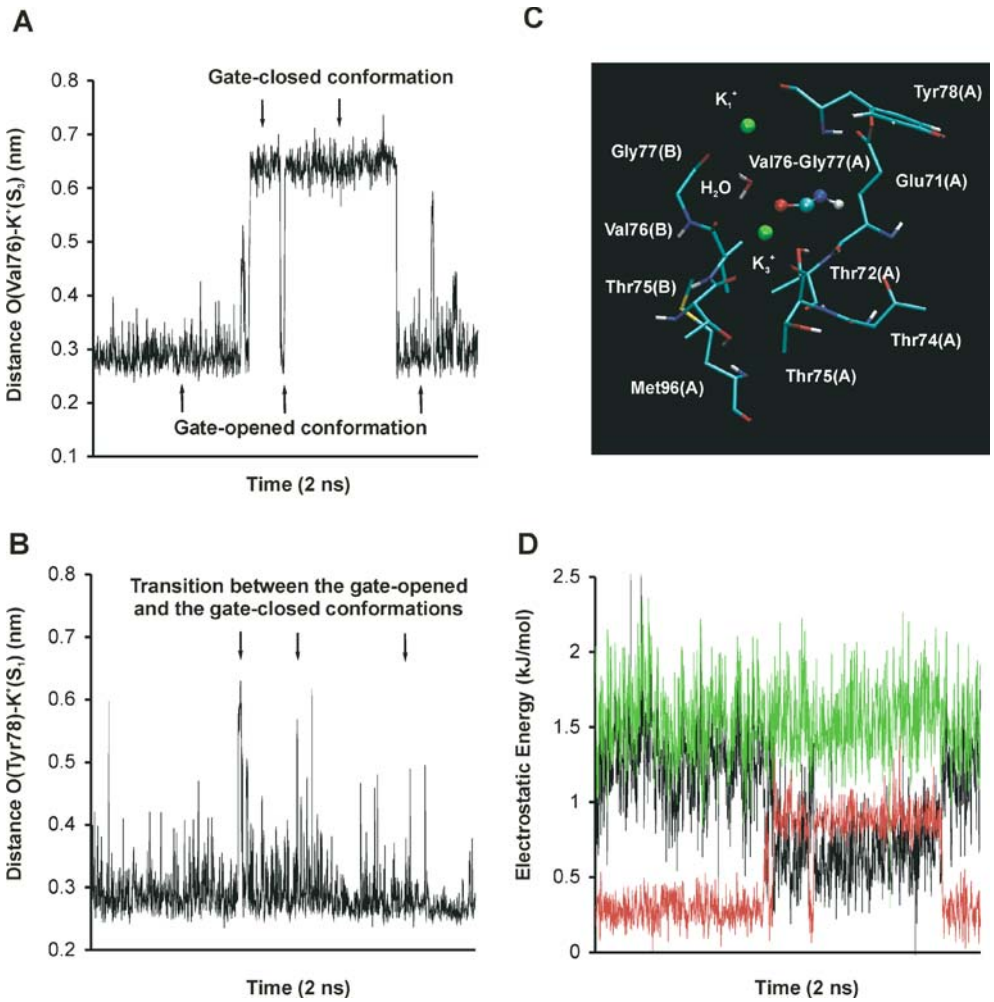

Fig. 3 (**A**) Distances between the carbonyl oxygen of Val76 (of subunit with the leaping Val76-Gly77 peptide linkage) and potassium ion bound at the S_3 site, and (**B**) between the carbonyl oxygen of Tyr78 and potassium ion bound at the S_1 site in the same subunit during the 2 ns classical MD simulation of the 1K_3K configuration. During the simulation the Val76-Gly77 peptide linkage switched between the gate-opened and gate-closed conformations several times. (**C**) Schematic drawing of the leaping Val76-Gly77 peptide linkage (*ball and stick*) and its local environments (*tube*) within ca 5 Å involved in calculations of the electrostatic energy. (**D**) The electrostatic energy between the leaping Val76-Gly77 peptide linkage and local environment (*red line*), and entire channel without the local environment (*black line*), and entire channel (*green line*). The energies are relative to an average Val76-Gly77-local environment electrostatic energy (−36.5 kJ/mol)

To investigate the reason of the stability of the flipped conformation, we plotted the potential electrostatic energy versus simulated time in 1K_3K (see Computational Details for more details). We find that this quantity does not change significantly upon flipping (Chart **D** in Fig. 3). However, plot of the electrostatic potential decomposed on local interactions shows that contributions of the residues within ca 5 Å from the carbonyl oxygen of Val76 play an important role for the stabilization of the gate-opened conformation of the selectivity filter of KcsA (Chart **D** in Fig. 3). In particular, crucial is the contribution of the K^+ ion bound at the S_3 site. On the other hand in the gate-closed conformation, a significant stabilization of the dipole is provided by the channel environment. Inspection of the single contributions shows that Thr75, Tyr78 and H_2O at the S_2 site play the most significant role in the stabilization of this conformation.

3.2 SMD simulations

To provide further insight on the gate-opened/gate-closed mechanism, we performed several sets of the SMD simulations with the steering velocity, $v = 0.03$ Å ps^{-1} (Table 1). By varying the force constant of the pulling spring ($f_1 = 2.4$, $f_2 = 3.1$ and $f_3 = 4.3$ kcal/mol $Å^2$) we evaluate here the effect on the permeation of

Table 1 Summary of the SMD simulations with the GROMOS 87 force field, steering velocity, $v = 0.03$ Å ps^{-1} varying force constant, $f_1 = 2.4$, $f_2 = 3.1$ and $f_3 = 4.3$ kcal/mol Å^2, respectively

Force const.	Number of trajectories	Starting state	Final state	Pulled group	Flux	VG flip
2.4	5	$S_1^{K+}S_3^{K+}S_{cav}^{K+}$	$S_{ext}^{K+}S_3^{K+}TS_{4cav}^{K+}$	$K^+(S_1)$	No	Yes
3.1	5	$S_1^{K+}S_3^{K+}S_{cav}^{K+}$	$S_{ext}^{K+}S_2^{K+}S_4^{K+}$	$K^+(S_1)$	Yes	No
4.3	5	$S_1^{K+}S_3^{K+}S_{cav}^{K+}$	$S_{ext}^{K+}S_2^{K+}S_4^{K+}$	$K^+(S_1)$	Yes	No

For every set five SMD simulations were performed with starting structures chosen from trajectory files of the equilibrium MD simulations. As indicated for the set with $f_1 = 2.4$ kcal/mol Å^2, the interconversion of the Val76-Gly77 peptide linkage occurred and no concerted movement of ions during pulling process was observed. In sets with larger force constants no change of the Val76-Gly77 linkage occurred and subsequent flux of ions toward extracellular side was observed

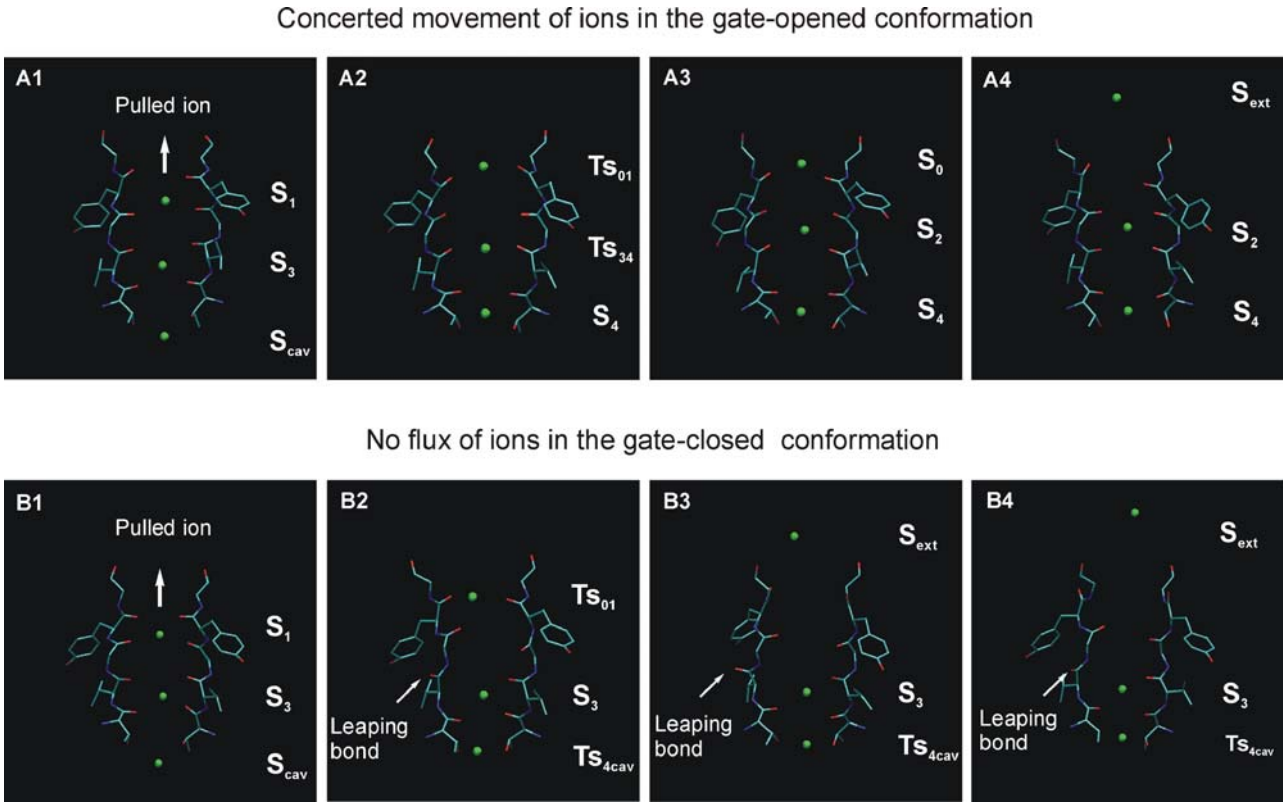

Fig. 4 Snapshots from steered MD simulations. The MD simulations with the pulling force costant, $f_3 = 4.3$ kcal/mol Å^2, indicate concerted movement of potassium ions from the cavity to extracellular solution when carbonyl oxygens of Val76 residues are positioned inside the selectivity filter (the gate-open conformation, snapshots A1–A4). In the case with a lower force constant, $f_1 = 2.4$ kcal/mol Å^2, the carbonyl oxygen of the Val76 residue in one subunit resides in a position leaped out from the selectivity filter (the gate-closed conformation, snapshots B1–B4) and no flux of ions was observed

the initial condition (Table 1) [47]. We pulled the potassium ion from the S_1 site into the extracellular solution, where a concerted movement of neighboring ions ($S_1^{K+}S_3^{K+}S_{cav}^{K+} \rightarrow S_0^{K+}S_2^{K+}S_4^{K+} \rightarrow S_{ext}^{K+}S_2^{K+}S_4^{K+}$) was observed (snapshots $A1 - A4$ in Fig. 4) in all five SMD trajectories with the f_2 and f_3 force constants. Thus, after the $S_1^{K+} \rightarrow S_0^{K+}$ transition, the ion in the cavity moved to the S_4 site, including in turn a movement of the neighboring ion from the S_3 to S_2 in the final step of the transition (a chart *B* in Fig. 5). We speculate that changes in the extracellular vestibule of the selectivity filter could induce a movement of ions at the opposite site of the filter, i.e., at the intracellular end of the filter.

For a smaller value of the force constant (f_1), the interconversion of the Val76-Gly77 peptide linkage bringing the channel into the non-conducting state was observed in all five SMD trajectories (Fig. 6): as a result, a K^+ ion remained in the S_3 site despite the vacancy of the S_2, S_1

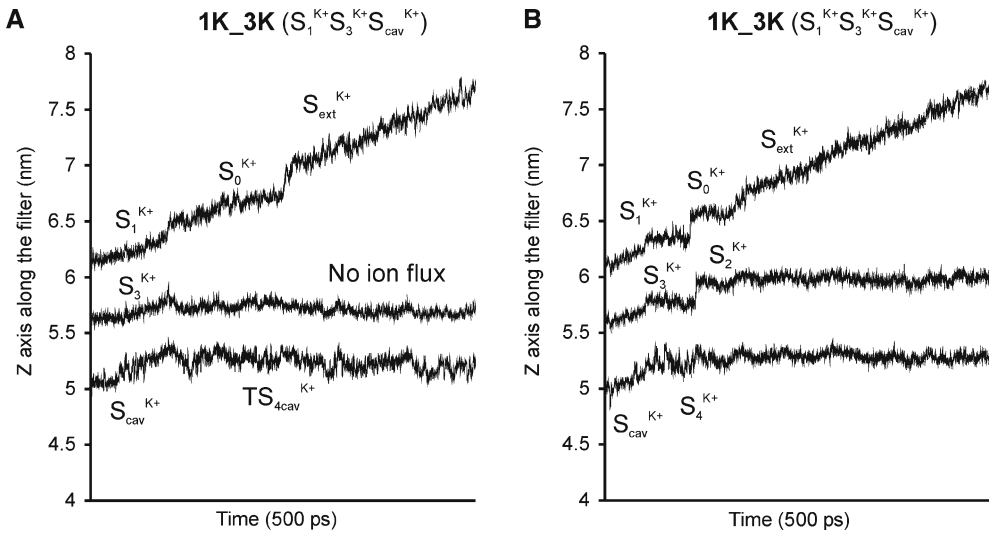

Fig. 5 Z coordinates of ions from trajectories of SMD simulations of both configurations: (**a**) the 1K_3K ($S_1^{K+}S_3^{K+}S_{cav}^{K+}$) configuration with $f_1 = 2.4$ kcal/mol Å^2 and (**b**) with $f_3 = 4.3$ kcal/mol Å^2 . No flux of ions is indicated in the SMD simulations with the gate-closed conformation of the filter (**a**)

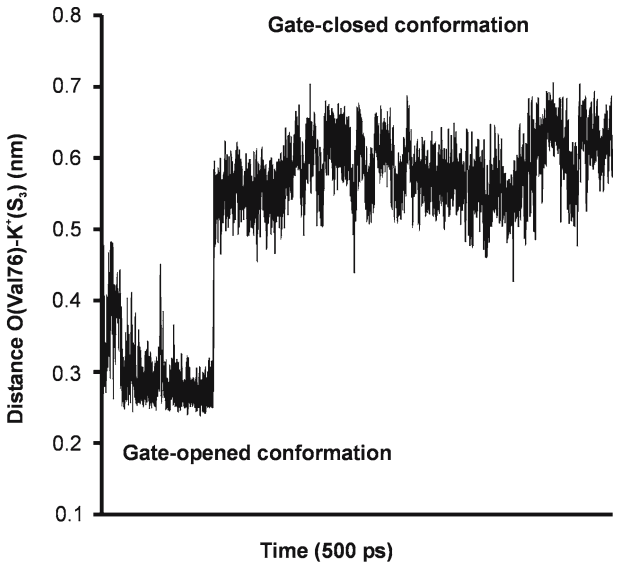

Fig. 6 Distances between the carbonyl oxygen of Val76 (of subunit with the leaping Val76-Gly77 peptide linkage) and potassium ion bound at the S_3 site during the 500 ps SMD simulation of the 1K_K3 configuration with the $f_1 = 2.4$ kcal/mol Å^2 . At the beginning of the simulation the Val76-Gly77 peptide linkage switched from the gate-opened to gate-closed conformation, at which the filter stayed until the end of the simulation

and S_0 sites (snapshots B2 – B4 in Fig. 4 and a chart A in Fig. 5). We did not observed in the non-conducting state any conformational change of the Thr75-Va76 peptide linkage as found by Berneche and Roux [13,14].

The reason for the dramatic differences between the SMD simulations with smaller and larger force constant could be in different kinetic properties of the pulled ion based on the initial pulling parameters. If the ion at the S_3 site starts to move toward S_2, ion–dipole interactions among potassium ion and four carbonyl oxygens of Val76 are strengthened, and subsequently the Val76-Gly77 linkage is stabilized at the gate-opened conformation (the SMD simulations with f_2 and f_3). If the ion transport is slower, the fast Val76-Gly77 conversion to the gate-closed conformation can take place in advance and the ion is temporarily blocked at the S_3 site until the filter switches to the gate-opened conformation (the SMD simulations with f_1). Thus, the Val76-Gly77 flip could be the origin of the so-called open channel noise, i.e., can be a source of fluctuations – possible present in most other ionic channels – not associated to fluctuations of the gating machinery at the inner side of the channel.

4 Conclusion

We have investigated mechanistic properties of ion permeation through the selectivity filter of the potassium KcsA channel using MD and SMD simulations. The MD simulations along with steered MD simulations carried out with GROMOS 87 force field pointed to two distinct state of the filter, the gate-opened and gate-closed conformations, were observed in the trajectories calculated. The conformations differ in positions of the carbonyl oxygen and amide nitrogen of the peptide bond between Val76 and Gly77 residues in one subunit of the channel. In the gate-opened conformation, the carbonyl oxygen is positioned toward the bound ion at the S_3 site and concerted movement of ions through the filter is observed. In the gate-closed conformation with the amide

nitrogen inside the selectivity filter, no ion flux was observed and one ion was subsequently blocked at the S_3 site during the simulations. These results have been already reported in a CHARMM-based MD simulations [13], although in previous work a concomitant conversion of the Thr75-Val76 linkage was also observed [14].

Novel information is here given on why such a transition can occur. The electrostatic potential energy of the Val76-Gly77 peptide linkage in the field of the channel is similar in both gate-opened and gate-closed conformations. In gate-closed conformation of the Val76-Gly77 peptide linkage the loss of the electrostatic interaction between the carbonyl oxygen of Val76 and K^+ ion is fully counterbalanced by the effect of the field of the channel and its environment. In particular, the Thr75, Tyr78 residues and H_2O at the S_2 position provide significant stabilization of the gate-closed conformation.

References

1. MacKinnon R (2003) Potassium channels. FEBS Lett 555: 62–65
2. Yellen G (1999) The bacterial K^+ channel structure and its implications for neuronal channels. Curr Opin Neurobiol 9:267–273
3. Yellen G (2002) The voltage-gated potassium channels and their relatives. Nature 419:35–42
4. MacKinnon R (2004) Potassium channels and the atomic basis of selective ion conduction (Nobel Lecture). Angew Chem Int Ed 43:4265–4277
5. LeMasurier M, Heginbotham L, Miller C (2001) KcsA: it's a potassium channel. J Gen Physiol 118:303–313
6. Heginbotham L, LeMasurier M, Kolmanova-Partensky L, Miller C (1999) Single Streptomyces lividans K^+ channels functional asymmetries and sidedness of proton activation. J Gen Physiol 114:551–559
7. Heginbotham L, Lu Z, Abramson T, MacKinnon R (1994) Mutations in the K^+ channel signature sequence. Biophys J 66:1061–1067
8. Doyle DA, Cabral JM, Pfuetzner RA, Kuo AL, Gulbis JM, Cohen SL, Chait BT, MacKinnon R (1998) The structure of the potassium channel: molecular basis of K^+ conduction and selectivity. Science 280:69–77
9. Zhou YF, Morais-Cabral JH, Kaufman A, MacKinnon R (2001) Chemistry of ion coordination and hydration revealed by a K^+ channel-Fab complex at 2.0 angstrom resolution. Nature 414:43–48
10. Morais-Cabral JH, Zhou YF, MacKinnon R (2001) Energetic optimization of ion conduction rate by the K^+ selectivity filter. Nature 414:37–42
11. Long SB, Campbell EB, MacKinnon R (2005) Crystal structure of a mammalian voltage-dependent Shaker family K^+ channel. Science 309:897–903
12. Berneche S, Roux B (2001) Energetics of ion conduction through the K^+ channel. Nature 414:73–77
13. Berneche S, Roux BI (2005) A gate in the selectivity filter of potassium channels. Structure 13:591–600
14. Berneche S, Roux B (2000) Molecular dynamics of the KcsA K^+ channel in a bilayer membrane. Biophys J 78:2900–2917
15. Roux B (2005) Ion conduction and selectivity in K^+ channels. Annu Rev Biophys Biomolec Struct 34:153–171
16. Roux B, Schulten K (2004) Computational studies of membrane channels. Structure 12:1343–1351
17. Roux B, Allen T, Berneche S, Im W (2004) Theoretical and computational models of biological ion channels. Q Rev Biophys 37:15–103
18. Domene C, Haider S, Sansom MS (2003) Ion channel structures: a review of recent progress. Curr Opin Drug Discov Dev 6:611–619
19. Domene C, Bond PJ, Sansom MSP (2003) Membrane protein simulations: ion channels and bacterial outer membrane proteins. Protein simulations. Academic Press Inc, San Diego p 159-+
20. Roux B (2002) Theoretical and computational models of ion channels. Curr Opin Struct Biol 12:182–189
21. Ash WL, Zlomislic MR, Oloo EO, Tieleman DP (2004) Computer simulations of membrane proteins. Biochim Biophys Acta-Biomembr 1666:158–189
22. Sansom MSP, Shrivastava IH, Bright JN, Tate J, Capener CE, Biggin PC (2002) Potassium channels: structures, models, simulations. Biochim Biophys Acta-Biomembr 1565:294–307
23. Berneche S, Roux B (2001) Mechanism of ions permeation in the KcsA potassium channel. Biophys J 80:175a
24. Noskov SY, Berneche S, Roux B (2004) Control of ion selectivity in potassium channels by electrostatic and dynamic properties of carbonyl ligands. Nature 431:830–834
25. Shrivastava IH, Sansom MSP (2000) Simulations of ion permeation through a potassium channel: Molecular dynamics of KcsA in a phospholipid bilayer. Biophys J 78:557–570
26. Shrivastava IH, Tieleman DP, Biggin PC, Sansom MSP (2002) K^+ versus Na^+ ions in a K channel selectivity filter: A simulation study. Biophys J 83:633–645
27. Domene C, Sansom MSP (2003) Potassium channel, ions, and water: simulation studies based on the high resolution X-ray structure of KcsA. Biophys J 85:2787–2800
28. Capener CE, Sansom MSP (2002) Molecular dynamics simulations of a K channel model: Sensitivity to changes in ions, waters, and membrane environment. J Phys Chem B 106:4543–4551
29. Capener CE, Shrivastava IH, Ranatunga KM, Forrest LR, Smith GR, Sansom MS (2000) Homology modeling and molecular dynamics simulation studies of an inward rectifier potassium channel. Biophys J 78:2929–2942
30. Domene C, Grottesi A, Sansom MS (2004) Filter flexibility and distorsion in a bacterial inward rectifier K^+ channel: simulation Studies of KirBac1.1. Biophys J 87:256–267
31. Luzhkov VB, Aqvist J (2000) A computational study of ion binding and protonation states in the KcsA potassium channel. Biochim Biophys Acta-Protein Struct Molec Enzym 1481:360–370
32. Aqvist J, Luzhkov V (2000) Ion permeation mechanism of the potassium channel. Nature 404:881–884
33. Allen TW, Kuyucak S, Chung SH (1999) Molecular dynamics study of the KcsA potassium channel. Biophys J 77:2502–2516
34. Berneche S, Roux B (2003) A microscopic view of ion conduction through the K^+ channel. Proc Natl Acad Sci USA 100:8644–8648
35. Biggin PC, Smith GR, Shrivastava I, Choe S, Sansom MSP (2001) Potassium and sodium ions in a potassium channel studied by molecular dynamics simulations. Biochim Biophys Acta-Biomembr 1510:1–9
36. Compoint M, Carloni P, Ramseyer C, Girardet C (2004) Molecular dynamics study of the KcsA channel at 2.0-angstrom resolution: stability and concerted motions within the pore. Biochim Biophys Acta-Biomembr 1661:26–39

37. Guidoni L, Torre V, Carloni P (1999) Potassium and sodium binding to the outer mouth of the K^+ channel. Biochemistry 38:8599–8604
38. Guidoni L, Torre V, Carloni P (2000) Water and potassium dynamics inside the KcsA K^+ channel. FEBS Lett 477: 37–42
39. Brooks BR, Bruccoleri RE, Olafson BD, States DJ, Swaminathan S, Karplus M (1983) CHARMM - a program for macromolecular energy, minimization, and dynamics. J Comput Chem 4:187–217
40. MacKerell AD, Bashford D Jr, Bellot M, Dunbrack RL, Evanseck JD, Field MJ, Fischer S, Gao HGJ, Joseph-McCarthy D, Ha S, Kuchnir L, Kuczera K, Lau FTK, Mattos C, Michnick S, Ngo T, Nguyen DT, Prodhom B, Reiher WE, Roux B, Schlenkrich M, Smith J, Stote R, Straub J, Watanabe M, Wiorkiewicz-Kuczera J, Karplus M (1998) All-atom empirical potential for molecular modeling and dynamics studies of proteins. J Phys Chem B 102:3586–3616
41. Jarzynski C (1997) Nonequilibrium equality for free energy differencies. Phys Rev Lett 78:2690–2693
42. Jarzynski C (1997) Equilibrium free-energy differences from nonequilibrium measurements: a master-equation approach. Phys Rev E 56:5018–5035
43. Hummer G, Szabo A (2001) Free energy reconstruction from nonequilibrium single-molecule pulling experiments. Proc Natl Acad Sci USA 98:3658–3661
44. Crooks GE (2000) Path-ensemble averages in systems driven far from equilibrium. Phys Rev E 61:2361–2366
45. Park S, Khalili-Araghi F, Tajkhorshid E, Schulten K (2003) Free energy calculation from steered molecular dynamics simulations using Jarzynski's equality. J Chem Phys 119:3559–3566
46. Isralewitz B, Gao M, Schulten K (2001) Steered molecular dynamics and mechanical functions of proteins. Curr Opin Struct Biol 11:224–230
47. Cascella M, Guidoni L, Maritan A, Rothlisberger U, Carloni P (2002) Multiple steering molecular dynamics applied to water exchange at alkali ions. J Phys Chem B 106:13027–13032
48. Vidossich P, Cascella M, Carloni P (2004) Dynamics and energetics of water permeation through the aquaporin channel. Proteins 55:924–931
49. Jensen MØ, Park S, Tajkhorshid E, Schulten K (2002) Energetics of glycerol conduction through aquaglyceroporin GlpF. Proc Natl Acad Sci USA 99:6731–6736
50. Monticelli L, Robertson KM, MacCallum JL, Tieleman DP (2004) Computer simulation of the KvAP voltage-gated potassium channel: steered molecular dynamics of the voltage sensor. FEBS Lett 564:325–332
51. Gross A, Columbus L, Hideg K, Altenbach C, Hubbell WL (1999) Structure of the KcsA potassium channel from *Streptomyces lividans*: a site-directed spin labeling study of the second transmembrane segment. Biochemistry 38:10324–10335
52. Berneche S, Roux B (2002) The ionization state and the conformation of Glu-71 in the KcsA K^+ channel. Biophys J 82:772–780
53. Ranatunga KM, Shrivastava IH, Smith GR, Sansom MSP (2001) Side-chain ionization states in a potassium channel. Biophys J 80:1210–1219
54. van Gunsteren WF, Berendsen HJC (1987) GROMOS 87 manual. Biomos BV Nijenborgh 4, 9747 AG Groningen, The Netherlands
55. Hermans J, Berendsen HJC, van Gunsteren WF, Postma JPM (1984) A consistent empirical potential for water-protein interactions. Biopol 23:1513–1518
56. Lindahl E, Hess B, van der Spoel D (2001) GROMACS 3.0: a package for molecular simulation and trajectory analysis. J Mol Model 7:306–317
57. Berendsen HJC, Vanderspoel D, Vandrunen R (1995) Gromacs – a message-passing parallel molecular-dynamics implementation. Comput Phys Commun 91:43–56
58. Berendsen HJC, Postma JPM, van Gunsteren WF, Dinola A, Haak JR (1984) Molecular-dynamics with coupling to an external bath. J Chem Phys 81:3684–3690
59. Aqvist J (1990) Ion water interaction potentials derived from free-energy perturbation simulations. J Phys Chem 94:8021–8024
60. Kaminski G, Duffy EM, Matsui T, Jorgensen WL (1994) Free-energies of hydration and pure liquid properties of hydrocarbons from the opls all-atom model. J Phys Chem 98:13077–13082
61. Berendsen HJC, Postma JPM, van Gunsteren WF, Hermans J (1981) Intermolecular forces reidel. Dordrecht
62. Darden T, York D, Pedersen L (1993) Particle mesh Ewald – an N.Log(N) method for Ewald sums in large systems. J Chem Phys 98:10089–10092
63. Hess B, Bekker H, Berendsen HJC, Fraaije J (1997) LINCS: a linear constraint solver for molecular simulations. J Comput Chem 18:1463–1472